Appl. Phys. B 66, 251–258 (1998)

Applied Physics B
Lasers
and Optics
© Springer-Verlag 1998

Effect of laser intensity and of lower-state rotational energy transfer upon temperature measurements made with laser-induced predissociative fluorescence

E.W. Rothe[1], **Y. Gu**[1], **A. Chryssostomou**[2], **P. Andresen**[3], **F. Bormann**[3]

[1] Department of Chemical Engineering and Materials Science, Wayne State University, Detroit, MI 48202, USA
(Fax: +1-313/5773810)
[2] Laser-Laboratorium Göttingen, Postfach 2619, D-37016 Göttingen, Germany
[3] Angewandte Laserphysik, Universität Bielefeld, Universitätsstraße 25, D-33615 Bielefeld, Germany

Received: 6 February 1997/Revised version: 28 July 1997

Abstract. Laser-induced predissociative fluorescence (LIPF) is often used to deduce gas temperatures from the relative populations of two rotational states. In this paper we present calculations, as well as a measurement, that show that the ratio of LIPF signals from those two states, and thus the deduced temperature, is sensitive to laser intensity. Even for an idealized situation without collisions, the deduced temperature can vary by a factor of two or three, although a careful calibration procedure will reduce or eliminate this error. However, rotational energy transfer (RET) collisions usually do occur in the lower state, and then the laser spectral intensity dependence of the fluorescence ratio can also depend heavily upon the value of the RET coefficients. Physical phenomena involve time-dependent values of the lower-state population, caused by competition between filling by RET and depletion by laser pumping. RET reduces the sensitivity of the observed signal to the laser's spectral intensity; however, the conversion of a measured fluorescence ratio to temperature is particularly difficult, because RET rates can be a function of local conditions and of the rotational state being populated. Furthermore, the spatial alignment of the excited-state molecules decreases at higher laser energies, which can also lead to large changes in the measured fluorescence ratio. We measured the ratio of fluorescence intensities that are induced by tunable KrF laser light via the A $\leftarrow$ X, 3 $\leftarrow$ 0 transitions $P_2(8)$ and $Q_2(11)$ in OH.

PACS: 32; 33; 42.30

Temperature measurements are often made using laser-induced fluorescence. Typically, the population ratio r of two rotational levels is deduced from the corresponding fluorescence intensities, and these intensities are converted to temperature via the Boltzmann relationship. The conversion involves various molecular spectroscopic constants (often well known), the fluorescence quantum yields of the excited state (usually not well known), and polarization parameters [1] (usually tricky to apply quantitatively). At higher pressures, for instance atmospheric, the conversion of such data to temperature can be complex because of collisional quenching of some upper-state molecules that would otherwise fluoresce. Laser-induced predissociative fluorescence (LIPF) considerably simplifies that problem [2] because the upper-state molecules dissociate within mean lifetimes τ_d that are so short [2–4] that there are almost no collisions. Then the relevant fluorescence quantum yield (i.e. the fraction of the laser-prepared upper state that fluoresces at the measured transitions) is approximately $A^*\tau_d$, where A^* is the sum of spontaneous emission rates for all measured transitions from the upper state. However, we will show that deduced temperatures are also strongly influenced by collisions in the lower state.

Laufer and co-workers [5–7] have discussed the necessity for calibration in LIPF temperature measurements. They excited the A $\leftarrow$ X, 3 $\leftarrow$ 0 transitions $P_2(8)$ and $Q_2(11)$ in OH with tunable KrF laser light [5]. The two lower states have $J'' = N'' - \frac{1}{2} = 7.5$ and 10.5 respectively, they have a precisely known energy level separation (1084 cm^{-1}), and have degeneracies $(2J'' + 1)$ [8]. We use the same two transitions here.

Let N_1 and N_2 be the populations in the upper and lower states respectively, and N_1^0 an initial (i.e. before the laser pulse) population. The ratio of initial populations is $r = N_1^0(8)/N_1^0(11)$, where 8 and 11 are the values of N''. The Boltzmann equation yields $T = 1560/\ln(11r/8)$. Unfortunately, as we will show below, the ratio of the measured fluorescence intensities R is a strong function of the laser's spectral intensity, and also of the rotational energy transfer (RET) rate to the two-probed, time-dependent populations $N_1(8)$ and $N_1(11)$. If we substitute R for r in the equation, T will change drastically in value, and a simple calibration will not avoid these problems.

1 Initial discussion

Now let us consider a CH_4-air flame at atmospheric pressure. With our LIPF process, the dissociation rate of A-state OH (i.e., $1/\tau_d$) is fast compared with its collision rate, usually to the rate of laser pumping back to the ground state, and to the spontaneous emission rate. Thus almost all of the A-state OH

dissociates without fluorescence. The probability that the OH molecules do fluoresce before dissociation is proportional to τ_d. We will discuss three cases that produce a change of the fluorescence intensity ratio R, and thus of apparent temperature, with laser spectral intensity.

1.1 LIPF with no rotational energy transfer

This case is applicable only at very low densities. Each fluorescence yield is still proportional to τ_d. First, consider a fixed small laser spectral intensity. Then the number of OH molecules excited to each upper state is proportional to B_i, the appropriate Einstein coefficient, and the constant populations (i.e. $N_i = N_i^0$) of the lower state i. The signal ratio R is proportional to r, the desired ratio of the initial populations, and also proportional to the ratios of the two B_i and of those of the τ_d. Next, consider a large spectral intensity (one that is often attained with common experimental conditions) where all OH molecules that constituted the two original ground-state populations [i.e. $N_1^0(8)$ and $N_1^0(11)$] are pumped out. In this spectral intensity range, the actual values of the B-factors, and of the laser spectral intensity, have no effect. Therefore, at large laser intensity, R becomes a constant that depends only on r and τ_d, with B and τ_d molecular constants, and this implies that the system can be calibrated.

1.2 LIPF with rotational energy transfer

In this case, the laser light pumps OH out of the ground state, but the RET processes tend to refill it. At small laser intensities, RET will be less important because it retains the two ground-state populations at nearly their original value. Then R is determined by roughly the same factors as the small-intensity case with no RET. At large laser intensities, the pumping rate for OH to an upper state is limited by that at which RET can supply ground-state OH molecules rather than the rate at which those are pumped up by the laser. We then have that R depends not only on the ratio r but also upon RET constants and the τ_d for each species. The RET rates, which may differ for the two ground states, are not molecular properties, which makes calibration difficult.

1.3 Polarization phenomena

Complications occur when a linearly polarized laser is used to excite two different branches [1]. We use a Q- and a P-excitation to analyze for $N_1^0(11)$ and $N_1^0(8)$ respectively. The Q-excitation occurs most efficiently when the laser light's $\boldsymbol{E}$ vector is parallel to the angular momentum vector of the OH, $\boldsymbol{J}_{OH}$. In contrast, the P-excitation works best when $\boldsymbol{E} \perp \boldsymbol{J}_{OH}$ In each case, then, molecules with certain spatial alignments relative to the $\boldsymbol{E}$ vector are preferentially removed from the bottom state, and certain upper-state alignments are preferentially formed. The particular distributions formed depend on the extent of pumping and the rate of RET collisions. Both factors refer to particular spatial alignments within the rotational levels. With a given detector, the efficiency of detection for an OH molecule also depends in turn upon its spatial alignment. For example, when the fluorescence involves a Q-transition, the OH is most efficiently detected when $\boldsymbol{J}_{OH}$ is perpendicular to a line between the OH molecule and the detector. That OH alignment, however, yields a minimum efficiency when P-branch fluorescence is measured.

Note that LIPF tends to have more pronounced polarization phenomena than normal LIF. This is because the upper state is nearly collision-free. Collisions degrade the nascent alignment distribution of the $\boldsymbol{J}_{OH}$ that is prepared by the laser.

2 Magnitude of RET effect

We will use Fig. 1, whose origin will be described later, to show the magnitude of the RET effect. It contains calculated ratios R of fluorescence signals as a function of laser spectral intensity I at an actual temperature of 2155 K. The ground-state RET-rate constant Q_{RET} is the parameter. We normalize the initial population $N_1^0(11)$ to be unity. At 2155 K, the Boltzmann equation predicts a 1.5-times larger population in $N'' = 8$, so that $N_1^0(8) = 1.50$. That yields $r = 1.50$, which is often used hereafter. The scale at the right of Fig. 1 shows temperatures that were calculated from $T = 1560/\ln(11R/8)$. This equation uses our calculated R rather than $r\,[\equiv N_1^0(8)/N_1^0(11)]$, the desired ratio of initial populations.

In the diagram of Fig. 1, we have plotted I from 0 to 200 MW/(cm^2 − cm^{-1}). By definition, $I \equiv E_p/(\tau\sigma\Delta\nu)$, where E_p is the laser pulse energy, and τ, σ and $\Delta\nu$, are the beam's pulse duration, its cross section, and its spectral width

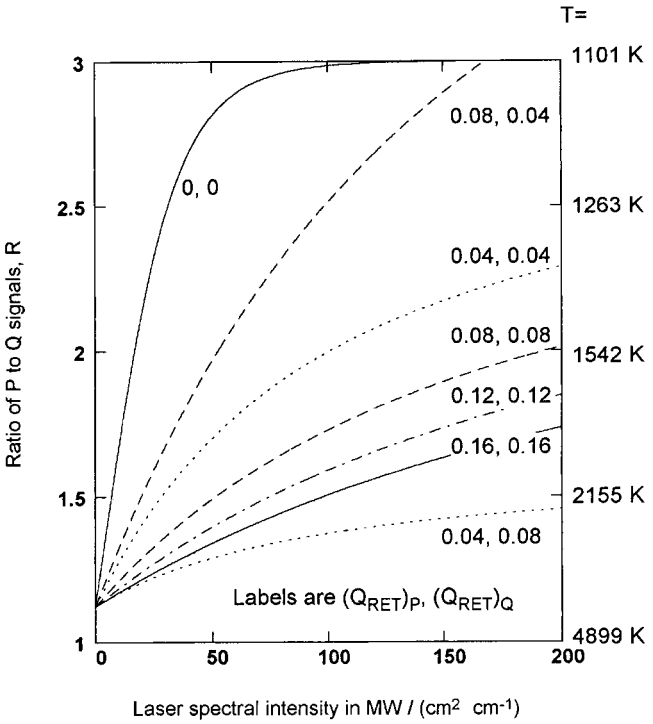

Fig. 1. The calculated ratio R of fluorescence intensities for various RET-rate coefficients for an actual temperature of 2155 K. A line labeled "m, n" means the line for those values m and n of Q_{RET8} and Q_{RET11} respectively, in units of 10^{10} s^{-1}. Under reasonable conditions (see text), the abscissa has a range of approximately 0–200 mJ/pulse. The apparent temperature scale at the right has been calculated from $T = 1560/\ln(11R/8)$: The correct temperature value would be obtained if R is replaced by r, the actual ratio of initial ground state populations. Here $r = 1.50$

respectively. In order convert I to the more common E_p, consider a fairly standard operation of a tunable KrF laser, i.e. $\tau = 13.3\,\text{ns}$, $\sigma = 1\,\text{mm} \times 10\,\text{mm}$, and $\Delta\nu = 0.75\,\text{cm}^{-1}$. For this condition, I in MW/(cm$^2-$cm^{-1}) is numerically equal to E_p in mJ/pulse.

The solid trace (labeled 0, 0) at the top left of Fig. 1 is for the case discussed above, when there is no RET into either of the two lower states. Its steep initial slope leads us to the conclusion that the deduced temperatures are very sensitive to laser spectral intensity. To illustrate this deduction, let us temporarily ignore the temperature scale in Fig. 1 and recalibrate by assigning the actual temperature of 2155 K to the $I = 0$ value (giving $R = 1.128$) with the laser beam parameters assumed in the previous paragraph. If we used the laser described in the previous paragraph, at 0.3, 1.0, and 2 mJ/pulse, apparent temperatures of 1825 K, 1398 K, and 1143 K, respectively, would be deduced. Similar considerations apply to pulse-to-pulse variations of I, as manifested in values of E_p or in the spectral widths. Because this sensitivity to I shown in the no-RET case is caused only by molecular parameters, suitable calibration techniques might be introduced. Unfortunately, this is only a hypothetical case, because some RET occurs in almost all applications.

The other traces in Fig. 1 have been calculated (see below) with RET coefficients Q_{RET} as parameters. We see that all the initial slopes are different from the no-RET case, and that they differ considerably among themselves. For each probed lower state, at any value of I, this change arises from the competition between pumping out with the laser and refilling with RET. The values of Q_{RET} are unlikely to be the same for each lower state because of the energy-gap laws. They will depend upon local conditions, such as the density, composition, and temperature of the gas, in other words on the severity and the number of various types of collisions, each of which can have its own temperature-dependent cross-section.

3 Our model and related calculations

3.1 Description of model

We have previously presented [9] coupled differential equations governing the time dependence of the normalized populations N_1 and N_2 in an LIPF process involving RET. There, we normalized N_1^0, the lower-state population prior to the laser pulse, to unity. For simplicity, we assume the same degeneracy in the upper and lower state. These equations are:

$$\frac{\mathrm{d}N_1}{\mathrm{d}t} = BI(N_2 - N_1) + (1 - N_1)\,Q_{RET}\,, \tag{1}$$

and

$$\frac{\mathrm{d}N_2}{\mathrm{d}t} = BI(N_1 - N_2) - N_2 L\,. \tag{2}$$

We use these equations for each transition. At $t = 0$, we set $N_2 = 0$, $N_1 = N_1^0 \equiv 1$ for $N'' = 11$, and $N_1^0 = r$ ($= 1.50$ here) for $N'' = 8$. Equations (1) and (2) have effective first-order rate constants Q_{RET}, BI, and L (in units of s^{-1}), where B is the Einstein coefficient and I is the spectral laser intensity (in units of watts/(cm$^2-$cm^{-1})). The rate constant for the laser pumping is BI, and that for RET from an OH bath (whose population is assumed to remain constant) into state 1 is Q_{RET}. The rate coefficient for total loss from state 2, other than that due to laser pumping, is $L \equiv A + Q_{total} + PD$, where A and Q_{total} are components for the radiative loss, and for the sum of all collisional losses (by means of electronic quenching, or by vibrational or rotational energy transfer), respectively, from state 2. The rate coefficient PD (called P in [9]) is that for predissociation. In this sum, A is completely negligible [10] so $L = Q_{total} + PD$. For a rectangular pulse shape, which is used here, exact solutions for $N_1(t)$ and $N_2(t)$ are found in [9]'s Appendix. Those solutions can be analytically integrated over t from 0 to τ, where τ is the pulse duration.

All calculations shown in the Figures were performed with complete analytical solutions to (1) and (2) or with their integrals. However, we will present some approximations so as to justify our previous physical descriptions of the main effects.

For these calculations, we use $B_{11} = 11.68$ and $B_8 = 4.393\,\text{s}^{-1}/[\text{W}/(\text{cm}^2-\text{cm}^{-1})]$ [10]. The predissociation rates PD_{11} and PD_8 are 1.04 and 0.51 (both $\times 10^{10}\,\text{s}^{-1}$) [3, 4]. There is some uncertainty in these PD values. In all cases considered here, $Q_{total} \ll PD$ and, for simplicity, we set the values of L_{11} and L_8 as 1.1 and $0.55 \times 10^{10}\,\text{s}^{-1}$. We could only estimate the value of Q_{total}, but it is so small as to cause little error in L. At $I = 200\,\text{MW}/(\text{cm}^2-\text{cm}^{-1})$, the values of $B_{11}I$ and $B_8 I$ are ≈ 0.23 and 0.09 (both $\times 10^{10}\,\text{s}^{-1}$) respectively. In order to compare with our data, we assume reasonable parameters for our CH_4-air flame at atmospheric pressure. These are a temperature of 2155 K and a set of Q_{RET} values from 0 to $0.16 \times 10^{10}\,\text{s}^{-1}$, which are somewhat less than the $0.18 \times 10^{10}\,\text{s}^{-1}$ that was previously used in [9] for an H_2-O_2 flame[1]. We assume the laser beam to be uniform in space, and to consist of a square pulse with $\tau = 13.3\,\text{ns}$. That time is chosen to be consistent with [9]. It has also been shown therein that there are only minor changes in the conclusions for more realistic temporal and spatial laser pulse shapes.

3.2 Increase of fluorescence intensity ratio R with laser intensity I (no RET)

The integrated fluorescence intensity F from each excitation transition is $A^*\langle N_2\rangle$, where A^* represents a sum of Einstein coefficients for all measured emissions and $\langle N_2\rangle$ is the average value of N_2. We obtain values for $\langle N_2\rangle$ from $\tau^{-1}\int N_2\,\mathrm{d}t$. Because the ratio of Einstein factors A_8^*/A_{11}^* is ≈ 1 [10], we take $R\,(\equiv F_8/F_{11})$ to be $\int N_2(8)\,\mathrm{d}t/\int N_2(11)\,\mathrm{d}t$. We calculated the functions $N_2(t)$ and these integrals from the analytic solutions of (1) and (2) [9]. Figure 2 contains $N_2(8, t)$ and $N_2(11, t)$ at three values of I. Note, as described in the figure caption, that the three sets of traces have different scales for N_2.

[1] RET rates: In [9], we used an H_2-O_2 flame to measure RET within the A-state of OH and found that the $Q_{RET(A\text{-state})} = 0.18 \times 10^{10}\,\text{s}^{-1}$. Essentially, we looked at the ratio of fluorescence intensities from the laser-created J' to those from $\Delta J' = \pm 1$ and ± 2. For lack of further information, we then assumed that $Q_{RET} = Q_{RET(A\text{-state})}$. In order to see the effect on $Q_{RET(A\text{-state})}$ from the change from the H_2-O_2 flame used in [9] to a CH_4-air flame, we repeated in Detroit the measurement and data-reduction method described in [9]. We used a premixed flame of CH_4 burning in natural air. The result was $Q_{RET(A\text{-state})} = 0.15 \times 10^{10}\,\text{s}^{-1}$.

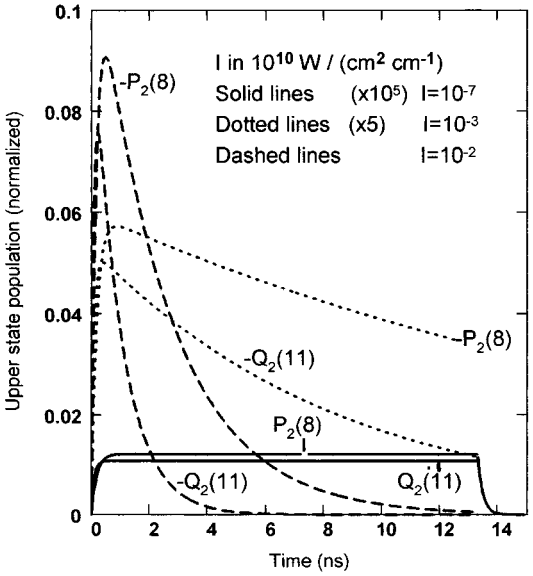

Fig. 2. The calculated time dependence of $N_2(8)$ and $N_2(11)$ for the $P_2(8)$ and $Q_2(11)$ transitions at three different values of the laser spectral intensity, all without RET. Note that the I labels use W, not MW in their units. The scale of the ordinate is correct for the dashed line, while those for the dotted and solid lines have been multiplied by 5 and 10^5 respectively. The value of $N_1(11)$ is normalized to be unity at $t = 0$. The plot is for $T = 2155$ K, so that the initial $N_1(8) = r = 1.5$. The small absolute values of the N_2 peaks are caused by laser-pumping rates that are small compared to the sum of predissociative and collisional losses from state 2. Only one of the traces displays an exponential decrease after the laser pulse

First consider laser intensities so small that only a negligible fraction of N_1^0 is pumped out. With $N'' = 11$ and $N_1 - N_2 \approx 1$, then (2) indicates that the initial slope of the curve is BI. As N_2 builds up, the increasing N_2L loss-term decreases the slope until it becomes zero. This is the solid trace in Fig. 2, corresponding to $I = 10^{-3}$ MW/(cm^2–cm^{-1}), and is labeled $Q_2(11)$. Then a steady state (SS) is reached when $N_2(\mathrm{SS}) = BI/L$, where $N_2(\mathrm{SS}) \ll 1$. Integration of (2) under these conditions yields $N_2(t) = [BI/L][1 - \exp(-Lt)]$. The exponential term represents the approach to $N_2(\mathrm{SS})$. The other solid trace, labeled $P_2(8)$, is for $N'' = 8$. It was calculated similarly but, in order to compare the populations, is multiplied by r (= 1.5 here). At the right of that solid trace, we show an exponential decrease of N_2 that occurs after the laser energy drops to zero. (We have omitted the analogous exponential decreases for other curves in Fig. 2 so as to avoid overlap.) The effect of these two exponentials cancels in the integration over time and leads to a value of $BI\tau/L$. Thus the ratio of the two signals is given by

$$R = r[L_{11}/L_8][B_8/B_{11}] = 1.128 \quad (3)$$
(for very small I, $Q_{\mathrm{RET}} = 0$) .

It is also visually obvious from the areas under each curve that $R > 1$.

The dotted lines in Fig. 2 apply for a spectral laser intensity of 10 MW/(cm^2–cm^{-1}) (of the order of 10 mJ), where a significant fraction of each ground state is pumped out. The maximum of $N_2(11, t)$ is greater than that of $[N_2(8, t)]/r$ ($r = 1.5$), because $[B_{11}I/L_{11}] > [B_8I/L_8]$. However, because $B_{11}I > B_8I$, $N_1(11, t)$ is depleted more rapidly than $N_1(8, t)$, and so $N_2(11, t)$ also declines more rapidly. The calculated value of R in this case is 1.67, and an inspection of the relative areas also shows that R has increased over its lower spectral intensity value.

Finally, the dashed lines in Fig. 2 apply for a spectral intensity another ten-times larger. The lines are similar to the dotted lines, except that both dashed lines are essentially zero by time τ. That means that the laser completely pumps out both ground states, and the number of OH radicals that are pumped to state 2 are proportional to the initial populations, with their fluorescence being proportional to L^{-1}. Then

$$R = F_8/F_{11} = rL_{11}/L_8 = 3 \quad (4)$$
(larger I, $Q_{\mathrm{RET}} = 0$) .

Thus, in accordance with these considerations, R rises from 1.128 to 3 and this behavior is shown in Fig. 1.

We now apply the approximation $BI \ll L$ to the analytic solutions in [9] and, after some algebra and integration, we obtain the simple result that

$$R \approx r[L_{11}/L_8][1 - \exp(-B_8I\tau)]/[1 - \exp(-B_{11}I\tau)] \quad (5)$$
($Q_{\mathrm{RET}} = 0$, approx.) .

Within a maximum deviation of 1.1%, this approximation reproduces the exact values for R that are plotted in Fig. 1. Equation (5) shows that the variation of R with I depends almost entirely upon the extent to which each ground state is depleted.

3.3 Effects of RET

Without RET, there is a reservoir of state-1 molecules that decreases with laser pumping. However, RET is a continuous source for state 1 and that weakens the I dependence of R, which, as was shown in (5) is caused primarily by the depletion of N_1. With RET, $N_1(t)$ quickly attains a steady state value $N_1(\mathrm{SS})$ that is determined primarily by the balance between molecules coming in via RET and those leaving via laser pumping [9]. Because BI is usually $\ll L$, only a negligible number of state-2 molecules are laser-pumped back to state 1 in most of our range. Our maximum value of BI is 0.23×10^{10} s^{-1}, while our smallest L is 0.55×10^{10} s^{-1}. Similarly, we obtain a dynamic equilibrium for $N_2(\mathrm{SS})$ between laser pumping in from the constant $N_1(\mathrm{SS})$ and the loss L out (mainly by predissociation). We can then set $\mathrm{d}N_1/\mathrm{d}t$ and $\mathrm{d}N_2/\mathrm{d}t$ equal to zero in (1) and (2) and solve the resulting algebra. This is an approximation because it ignores the initial deviation of $N_2(\mathrm{SS})$ from $N_2(t)$. Some algebraic manipulation shows that

$$R = r[L_{11}/L_8]\frac{L_{11}^{-1} + Q_{\mathrm{RET11}}^{-1} + (B_{11}I)^{-1}}{L_8^{-1} + Q_{\mathrm{RET8}}^{-1} + (B_8I)^{-1}} \quad (6)$$
($Q_{\mathrm{RET}} \neq 0$, approx.)

In our example the L^{-1} terms in the sum are small. At very low BI as well, (6) reduces to

$$R = r[L_{11}/L_8][B_8/B_{11}] = 1.128 \quad (7)$$
(for very small I, $Q_{\mathrm{RET}} \neq 0$) .

Equation (7) is identical to (3), because the RET rates are sufficient to keep $N_1(11, \mathrm{SS}) \approx N_1^0(11)$ and $N_1(8, \mathrm{SS}) \approx N_1^0(8)$. However, at larger intensities the Q_{RET} and BI terms become comparable and the $N_1(\mathrm{SS})$ attains smaller values.

Similarly we get from (6) for large laser energy

$$R = rN_2(8, \mathrm{SS})/N_2(11, \mathrm{SS}) = [L_{11}/L_8][Q_{\mathrm{RET8}}/Q_{\mathrm{RET11}}] \quad (\text{for} L \gg Q_{\mathrm{RET}} \text{ and } BI \gg Q_{\mathrm{RET}}), \tag{8}$$

and $R = 3$ for our example when $Q_{\mathrm{RET8}} = Q_{\mathrm{RET11}}$. In this high-energy limit, which is beyond the range of Fig. 1, the values of Q_{RET} in (8) have taken the place of the B in (7). This means that it is the RET rather than the laser pumping that is the rate-determining step for pumping from state 1 to state 2.

Figure 1 shows that the low I limit is satisfied, while the upper limit is approached when $BI \gg Q_{\mathrm{RET}}$. While at high laser energies (beyond the range of our KrF laser) the spectral intensity dependence of the ratio (and of deduced temperature) vanishes, and it is now directly dependent on the unknown ratio of $Q_{\mathrm{RET8}}/Q_{\mathrm{RET11}}$. Thus in Fig. 1, when $Q_{\mathrm{RET8}} = Q_{\mathrm{RET11}}$, we see the least I dependence when Q_{RET} is greatest, i.e. when $N_1(8, \mathrm{SS})$ and $N_1(11, \mathrm{SS})$ are at a maximum. Note that two more drastic cases exist when $Q_{\mathrm{RET8}} \neq Q_{\mathrm{RET11}}$, so that $N_1(8)$ and $N_1(11)$ are filled at different rates.

3.4 Effects of polarization

The discussion above assumes that the values of the L, BI, and Q_{RET} coefficients are independent of the spatial alignment of the OH molecules. That is true for L. However, a linearly polarized laser preferentially excites OH molecules that have particular spatial alignments with respect to the laser beams's $\boldsymbol{E}$ vector. Almost all of the resulting excited molecules dissociate. That leaves a non-isotropic reservoir of state-1 molecules. Equation (1) has a term $(1 - N_1)Q_{\mathrm{RET}}$ for the rate of RET into state 1. If we divide state 1 into substates according to their alignment, there should be different steady-state populations for each.

Doherty and Crosley [1] have discussed polarization effects in LIF and their influence upon measured relative intensities of P, Q, and R emissions. Their quantitative results apply under collision-free conditions. They also discuss the effects of collisions, but only for normal (i.e. non-predissociative) LIF. The much shorter upper-state lifetimes with LIPF makes the effects of collisions qualitatively different from those in normal LIF.

As will be described below, we did experiments in which the laser beam's $\boldsymbol{E}$ vector was perpendicular to the fluorescence path to the detector. Excitations were made with the $(3 \leftarrow 0)$ $P_2(8)$ and $Q_2(11)$ transitions. The detector measured only the corresponding emitted Q-lines, i.e., the $(3 \rightarrow 2)$ $Q_2(7)$ and $Q_2(11)$. When this experiment was performed, we did not consider that this choice of excitation and emission lines would lead to worst-case polarization effects. It does, however, afford an opportunity to illustrate potential difficulties.

For either LIF or LIPF, a pictorial explanation of the effects of the resulting polarization can be obtained from a well established classical approach [11]. In this picture, the transition dipole, for either a Q-excitation or a Q-emission, is parallel to the OH molecule's angular momentum vector $\boldsymbol{J}_{\mathrm{OH}}$, i.e. it is perpendicular to the molecule's plane of rotation. Thus, in a Q-excitation and a Q-emission, the two corresponding dipoles are parallel and, in the absence of collisions, remain fixed in space. The probability of exciting an OH is proportional to $\cos^2\theta$, where θ is the angle between its $\boldsymbol{J}_{\mathrm{OH}}$ and $\boldsymbol{E}$. Thus, with weak pumping, the emission dipoles have a $\cos^2\theta$ distribution about $\boldsymbol{E}$.

In our experimental arrangement, that maximizes the detected fluorescence. The light has intensity components whose polarization is parallel $I_\parallel$ and perpendicular $I_\perp$ to the $\boldsymbol{E}$ vector. A classical calculation [11] shows that $I_\parallel/I_\perp = 3$. (This classical result may be compared with $I_\parallel/I_\perp = 2.98$, which, at $J = 10.5$, is the quantum mechanical value [1, 11].) Without RET, large values of BI will pump out most of the X-state so that there is no longer a $\cos^2\theta$ distribution in the A-state, and this means that $I_\parallel/I_\perp$ will be much reduced. RET will tend to re-establish the original random alignment of OH in the X-state. The effect of collisions, and of predissociation upon $I_\parallel/I_\perp$ was discussed and measured in [9]. A major result there is that $I_\parallel/I_\perp$ decreases with increasing BI, mainly because the RET rate becomes too small to repopulate fully all those OH alignments in the X-state that were preferentially pumped out by the laser. A value of $I_\parallel/I_\perp < 3$ means less light reaches the detector, because the emission dipoles are less favorably aligned.

With a P-excitation and a Q-emission, there are two differences from the $Q - Q$ scheme. First, the P-transition dipole is perpendicular to $\boldsymbol{J}_{\mathrm{OH}}$. Thus, because it rotates with the molecule, the degree of alignment of the prepared A-state is reduced from that obtained with the Q-excitation. Secondly, the absorption and emission dipoles are mutually perpendicular. Thus with the same setup as above, $I_\parallel/I_\perp = \frac{1}{2}$ classically [11] and, at $J = 7.5$, is 0.58 quantum mechanically [1, 11]. Then, with weak pumping and no collisions, the fluorescence signal is at a minimum, and the fraction of light detected will increase with increasing BI.

The net result is that a measured ratio R $(= F_8/F_{11})$ of LIPF signals will increase with BI, as a result of changes in both components, until the alignment becomes completely random, and R will then reach a constant value. These collision-sensitive efficiencies cannot be dealt with by a calibration at a single value of the laser spectral intensity. However, if the ratio of $I_\parallel/I_\perp$ is measured at each value of laser spectral intensity [9], the value of R can be corrected. This was not done in the measurements to be described; however, in our subsequent analysis we will assume it has been done, and thus neglect the polarization effect.

In addition to the intensity changes described above, the effect of changes in the value of $I_\parallel/I_\perp$ upon the detection efficiency should also be considered. For example, when using a spectrometer, the grating efficiency is polarization-sensitive. This problem can often be solved experimentally: polarized light can easily be converted from linear to circular prior to reaching polarization-sensitive elements in the detection chain.

4 Experiments illustrating predicted effects

The experiments to be described below illustrate the rise of R with I. Both the normal RET description (see Fig. 1) and the polarization analysis predict this result. Which proportion of

each effect produced the observed result could not, however, be determined.

The experiments were completed in Göttingen and the model was subsequently developed in Detroit, with no initial interaction. Accordingly, the data are not suited for quantitative comparison. Nevertheless, they show the qualitative behavior predicted by the model. Because the experiments have been described in detail elsewhere [12], we provide only a summary here.

The OH was in a conical laminar flame with a diameter of ~ 1 cm. It was fueled by a stoichiometric mixture of CH_4 and synthetic air. A Lambda Physik tunable excimer laser EMG160-MSC was operated with KrF, and it had been modified for single-pass operation as described elsewhere [13]. The laser beam pulses were linearly polarized, had $0.73\,\mathrm{cm}^{-1}$ spectral width, and were 20 ns long. The beam was focused by a one-meter FL lens having a cross-section of $2 \times 3\,\mathrm{mm}^2$ within the flame. This corresponded to $I \approx 170\,\mathrm{MW/(cm^2}$–$\mathrm{cm^{-1}})$ at a maximum beam energy of 150 mJ/pulse. The beam passed through the peak of the conical flame front.

Part of the fluorescence from the flame was focused into an imaging spectrograph that had an intensified CCD in its exit plane. The beam's ***E*** vector was perpendicular to the direction of fluorescence observation, which maximized the measured fluorescence from Q-excitation. Details of the methods for mitigation of laser-spectral intensity variation, data acquisition, background subtraction, precision, intensity variation with wavelength and location, etc., are presented in [12].

Here we present a brief rationale for the original, but poor, choice of the particular spectral lines measured. They were a poor choice because of the very large polarization effects. In spite of predissociation of the $v' = 3$ states, some vibrational energy transfer (VET) does occur within the upper electronic state [1, 14] to the much longer-lived $v' = 0$, 1, or 2 states. With CH_4 and air, it has been shown [14] that more light comes from these states than from the desired $v' = 3$. Accordingly we chose to measure only the $3 \rightarrow 2$ fluorescence, consisting of a triplet of P, Q, and R lines. There was also a continuum of interfering fluorescence from unknown species. Because the Q-emission was found to be more intense than that from P or R, and we wished to maximize the ratio of OH signal to the continuum emission, the Q-line intensities were used for the temperature ratios.

The experimental data are shown in Fig. 3. They are plotted both as actual intensities for each transition (a) and for their ratio (b). Both individual plots look fairly linear, but we must note here that apparent linearity of the fluorescence intensities with laser energy does not mean that all is well! In [12], for instance, these data were fitted to find a value of Q_{RET}, and clearly the general shape in [12]'s Fig. 7 is in qualitative agreement with the behavior in our Fig. 1; however, the fit produced values for Q_{RET} in the range 0.001–$0.003 \times 10^{10}\,\mathrm{s}^{-1}$ which are unrealistically small values. The error is almost surely in the failure to take account of the drastic changes in the measured intensity ratios caused by the polarization effects previously discussed herein. Because Q_{RET} is a sum of all RET coefficients ΔQ_{RET} for particular OH alignment states, it is clear that $\Delta Q_{\mathrm{RET}} < Q_{\mathrm{RET}}$. We have no way of correcting our data for these phenomena.

However, our failure to reproduce this curve quantitatively, which is caused by the two different effects of RET collisions, should not obscure the major message of this paper: there is a large, experimentally observed change in the intensity ratio with laser energy.

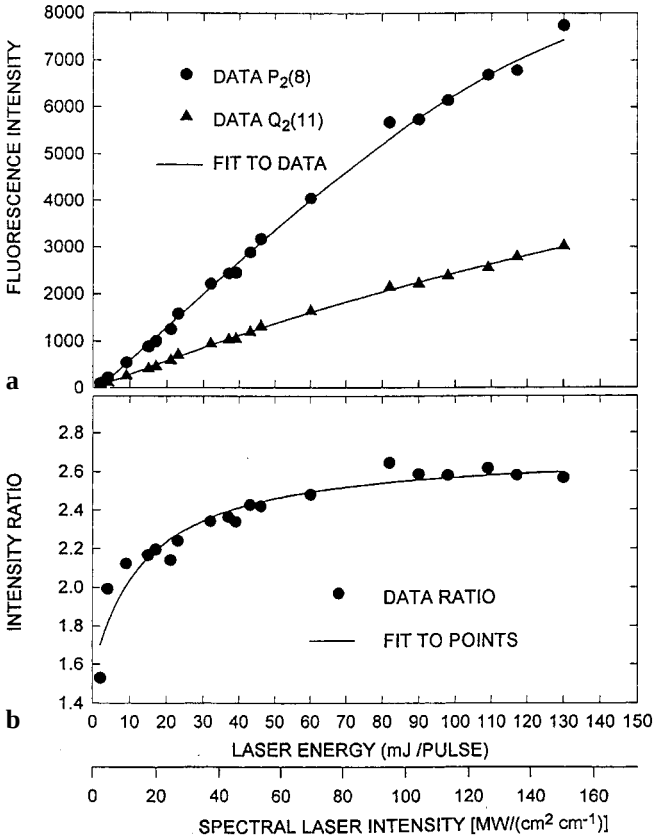

Fig. 3. a Experimental fluorescence intensities from a CH_4-air laminar flame resulting from $P_2(8)$ and $Q_2(11)$ excitations as a function of laser energy and of I, as well as a fit to those data. Each point is an average from 200 laser shots. **b** Ratio of the two data sets from the upper panel

5 Temperature determination with LIPF

5.1 Extrapolation to low I

It is tempting to measure fluorescence ratios at large laser intensities. The resulting large signals found there, which arise mainly from RET within the ground vibrational state, will enhance precision (but not necessarily accuracy). Unfortunately, as has been seen above, the magnitudes of the observed signals are heavily dependent upon the values of Q_{RET8} and Q_{RET11}, which are different for each environment and are probably different [15] for the two measured transitions.

The effect of the polarization errors discussed here can be drastically reduced by better choice of exciting and detected lines. They can be eliminated if the degree of polarization of the laser light is measured and the signals appropriately corrected. Accordingly, we focus on the low laser energy data as interpreted via (7). This equation contains only the B_{11}, L_{11}, B_8, and L_8 variables. While $L \equiv A + Q + PD$, and Q is collision-dependent, in our example $Q \ll PD$ and so contributes little to L. That means we may regard both B and L as molecular constants.

The low I portions of all the traces in Fig. 1 have a limit of $R = 1.128$, at $I = 0$. They have different initial slopes, depending on the values of Q_{RET}, but all are nearly straight lines. We suggest below extrapolation of values of R from finite values of I to $I = 0$. The values of the molecular constants determine the value of the intercept (see (7)). Thus, based on Fig. 1, we suggest the following:

1. Perform a calibration measurement at a known temperature such as that of Quagliaroli et al. [5]. Measure the fluorescence intensity ratio at several small values of the spectral laser intensity I. Make sure that the variation in E_{p} is made in such a way that other beam characteristics, such as cross-section or spectral width, are not affected.
2. Plot the resulting ratio of P-to-Q fluorescence versus I, and then extrapolate the results to zero laser spectral intensity. This will provide an overall calibration, independent of the RET rate as well as of the other calibration factors discussed by Quagliaroli et al.
3. Repeat this procedure in the medium to be diagnosed. A different slope may be obtained, but it is the extrapolated intercept that matters and that is independent of RET.
4. In principle, the method should be the most accurate using points with the lowest I. Unfortunately, that is where the measurement precision is least, and some compromise will have to be reached.

6 Ps-range laser pulses

The use of short-pulse lasers may largely avoid the effect of RET upon temperature measurement. Recent reports [16, 17] discuss some results and provide references. A detailed calculation should be done for any specific case, but some generalities will be mentioned here.

The work in [17] discussed the measurement of OH density via excitation to $v' = 2$, a non-predissociative state. However they used a 0.4 ns gate width on the detector, which yields results similar to short-lived upper states. Their laser had 100 MW/(cm^2–cm^{-1}), which is the middle of the range of Fig. 1, and a $\tau = 0.47$ ns pulse width.

Figure 4 displays our calculated $N_2(t)$ for a hypothetical case in which we use the same two transitions to predissociative states that have been considered in the rest of this paper, with a $\tau = 0.47$ ns square laser pulse. The $N_2(8)$ and $N_2(11)$ without RET, i.e. the solid lines, are a blowup of the dashed lines in Fig. 2 up to τ. There is an $\exp[-L(t-\tau)]$ decrease for $t > \tau$. We can see, first, that the effect of the finite Q_{RET} has relatively little effect on the areas under the curve; secondly, that the $N_2(11)$ is more affected than the $N_2(8)$ because, even in the short pulse time, there is more depletion of N_1; thirdly, that the area under the exponential tails is not negligible; and, fourthly, a look at the dashed lines in Fig. 2 shows that a large fraction of the probed state is involved in this analysis.

The additional use of a gate, such as the 0.4 ns one mentioned above, would allow added flexibility in selecting a desired portion of the curve.

7 Conclusions

Great care must be taken when converting ratios of LIPF data into temperatures. Even at low laser energies, significant temperature errors can occur from errors in measuring laser spectral intensity. The neglect of the effect of rotational energy transfer can lead to large errors. The system cannot be well calibrated unless accurate values for Q_{RET} are available for both states. Careful attention must also be paid to polarization effects, which require even more detailed knowledge of collisions, i.e. their paths into defined alignment states.

While RET leads to much higher signals than would otherwise occur, these signals are difficult to interpret. They are dependent on location and on state-sensitive rate constants. Calibration can be performed only for laser pumping that is sufficiently small that RET can maintain the original population of state 1. An alternative solution is to reduce the laser pulse length so that only a few molecules can flow into the ground state via RET during the time the laser is on.

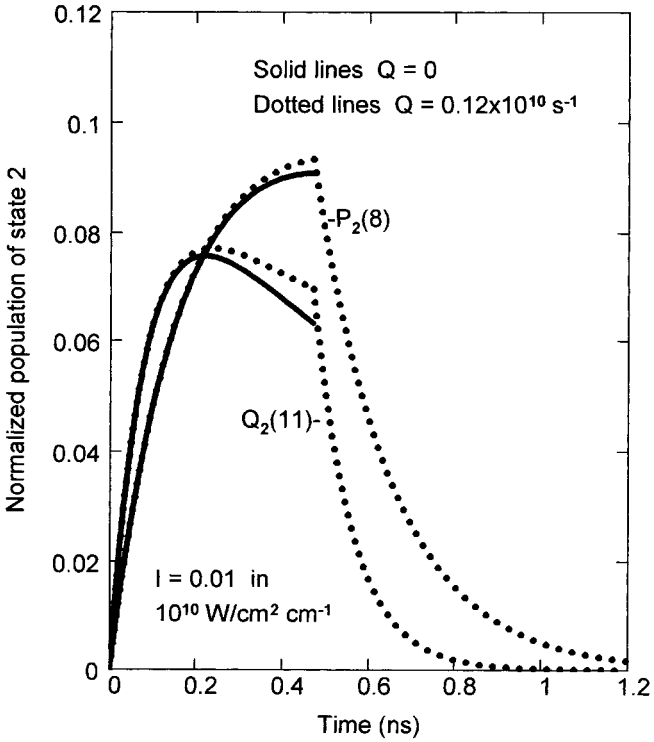

Fig. 4. The calculated time dependence of the densities $N_2(8)$ and $N_2(11)$ for the $P_2(8)$ and $Q_2(11)$ excitations with a laser pulse of 0.47 ns, i.e. a hypothetical ps-range laser. Compare these results with the dashed line in Fig. 2. The solid lines are without RET, the dotted lines with $Q_{\mathrm{RET8}} = Q_{\mathrm{RET11}} = 0.12 \times 10^{10}$ s^{-1}. Note from the areas under the respective curves that the influence of RET upon the fluorescence ratio is small, but still finite

Acknowledgements. We thank the National Aeronautics and Space Administration (Grant NAG3-1800) for partial support of this work. ER also thanks Professor H. Pauly, Director at the Max-Planck-Institut für Strömungsforschung, Göttingen, for the hospitality of his Institute, where some of the work was done. We are grateful to David Crosley for sending us appropriate A and B values for OH.

References

1. P.M. Doherty, D.R. Crosley: Appl. Opt. **23**, 713 (1984)
2. P. Andresen, A. Bath, W. Gröger, H.W. Lülf, G. Meijer, J.J. ter Meulen: Appl. Opt. **27**, 365 (1988)
3. J.A. Gray, R.L. Farrow: J. Chem. Phys. **95**, 7054 (1991)

4. D.E. Heard, D.R. Crosley, J.B. Jeffries, G.P. Smith, A. Hirano: J. Chem. Phys. **96**, 4366 (1992)
5. T.M. Quagliaroli, G. Laufer, J.C. McDaniel: Appl. Phys. B **59**, 635 (1994)
6. G. Laufer, T.M. Quagliaroli, R.H. Krauss, R.B. Whitehurst III, J.C. McDaniel, Jr., J.H. Grinstead: AIAA J. **34**, 463 (1996)
7. H. Grinstead, G. Laufer, J.C. McDaniel, Jr.: Appl. Opt. **34**, 5501 (1995)
8. J.A. Coxon: Can. J. Phys. **58**, 933 (1980)
9. E.W. Rothe, Y. Gu, G.P. Reck: Appl. Opt. **35**, 934 (1996)
10. J. Luque, D.R. Crosley, Chemical Physics Laboratory, SRI International, Menlo Park, CA, 94025 (personal communication 1994)
11. P.P. Feofilov: *The Physical Basis of Polarized Emission* (Consultants Bureau, New York 1961)
12. A. Chryssostomou: *Ortsaufgelöste Temperaturmessung mit laserinduzierter Prädissoziationsfluoreszenz in turbulenter Verbrennung*, doctoral dissertation, Bielefeld University (Cuvillier Verlag, Göttingen 1995)
13. G. Grünefeld, P. Andresen, H. Schlüter, E.W. Rothe: Appl. Phys. B **62**, 241 (1996)
14. K.L. Steffens, J.B. Jeffreys, D.R. Crosley: Opt. Lett. **18**, 1355 (1993)
15. M. Islam, I.W.M. Smith, J.W. Wiebrecht: J. Chem. Phys. **103**, 9676 (1995)
16. M.D. Burrows, F. Bormann, P. Andresen: Appl. Phys. B **61**, 451 (1995)
17. F. Bormann, T. Nielsen, M. Burrows, P. Andresen: Appl. Phys. B **62**, 601 (1996)